



Understanding eruptive style variations at calc-alkaline volcanoes: the 1913 eruption of Fuego de Colima volcano (Mexico)

S. Massaro^{1,2} · R. Sulpizio^{1,2} · A. Costa³ · L. Capra⁴ · F. Lucchi⁵

Received: 8 November 2017 / Accepted: 29 May 2018 / Published online: 26 June 2018
© Springer-Verlag GmbH Germany, part of Springer Nature 2018

Abstract

The 1913 sub-Plinian eruption of Fuego de Colima volcano (Mexico) occurred after almost 100 years of effusive and (minor) Vulcanian explosive activity, which modulated dome growth and destruction. Dome extrusion persisted from 1869 to 1913. The transition to explosive eruption started on 17 January 1913, and it progressed in three phases: (1) opening, with the generation of block-and-ash flows, (2) vent clearing, with strong explosions that destroyed the summit dome and decompressed the magmatic system, and (3) sustained column (sub-Plinian fallout) with final collapse producing pyroclastic density currents. Because of this succession of events, the 1913 activity represents an excellent case-study for investigating the eruptive style changes at calc-alkaline volcanoes. We investigated the conditions that led to eruptive style transition from effusive (dome growth) to explosive (the final sub-Plinian fallout) through steady-state numerical simulations, using subsurface data and independently inferred (from volcanological data) mass discharge rates as constraints. Results show good matches for hybrid geometrical settings of the shallow conduit-feeding system (i.e., dyke developing into a shallower cylindrical conduit), and the magma chamber top at 6 km of depth. The fragmentation level was shallower than 2 km, as inferred from the lithics contained in the sub-Plinian fall deposits of Phase (3). The most likely solution is represented by a dyke having major axis between 200 and 2000 m and the minor axis of 40 m. The dyke-cylinder transition was set at a depth of 500 m, with a cylinder diameter of 40 m. It emerges that at least two main mechanisms may be responsible for the effusive to explosive transition that led to the Phase (3) of the 1913 eruption: (i) an increase in magma chamber overpressure (magmatic triggering) or (ii) decrease of lithostatic stress acting on the volcano (non-magmatic triggering). The former implies arrival into the magma chamber of a batch of fresh magma, which can have volume between 10 and $200 \times 10^6 \text{ m}^3$, depending on the values of magma and host rock compressibility. The latter requires decompression-induced emptying of at least the equivalent of 1000 m of the magma column to produce the necessary unloading of the conduit-feeding system. A sudden jerk in the lateral spreading of the Fuego de Colima cone would be a reliable mechanism for decompressing the upper conduit and driving fragmentation processes over a time period of few hours. The results are not conclusive on an internal (magma chamber overpressure), external (lowering of lithostatic load), or mixed (internal and external) trigger of the observed eruptive style transition. This work highlights how different processes can have non-linear cascade effects on close-to-equilibrium volcanic systems like Fuego de Colima volcano.

Keywords Eruption dynamics · Effusive-explosive transition · Conduit-feeding system · Volcano spreading · Magma-rock interaction · Steady-state numerical model

Editorial responsibility: R. Cioni

✉ S. Massaro
silvia.massaro@idpa.cnr.it

¹ Dipartimento di Scienze della Terra e Geoambientali, Via Orabona 4, 70125 Bari, Italy

² IDPA-CNR, Via Roberto Cozzi 53, 20125 Milan, Italy

³ Istituto Nazionale di Geofisica e Vulcanologia, Via Donato Creti 12, 40128 Bologna, Italy

⁴ Centro de Geociencias UNAM, Campus Juriquilla, Santiago de Queretaro, Queretaro, Mexico

⁵ Dipartimento di Scienze Biologiche, Geologiche e Ambientali, Piazza di Porta S. Donato 1, 40126 Bologna, Italy

Introduction

Eruptive style transitions are frequently observed at many volcanoes around the world (e.g. Hildreth and Fierstein 2000; Sigmundsson et al. 2010; Nicholson et al. 2011; Sulpizio et al. 2016). In particular, eruptions involving the formation of lava domes can show recurrent transitions to Vulcanian explosive eruptions, and occasionally to sub-Plinian and even Plinian events. Examples include Unzen (Nakada et al. 1999), Mount St. Helens (Swanson and Holcomb 1999), Santiaguito (Williams and Self 1983), Lascar (Melnik et al. 2008), Fuego de Colima (Saucedo et al. 2010) and Soufrière Hills (Sparks and Young 2002) volcanoes. Changes in eruptive style imply variations in magma flow dynamics, which may mirror modifications in the driving pressure or conduit geometry (Woods and Koyaguchi 1994; Melnik and Sparks 2002; Costa et al. 2009a; Massaro et al. 2018). Changes in magma composition (induced by magma mixing; Woods and Cowan 2009; Nicholson et al. 2011) and rheology (driven by volatile-dependent crystallization; Melnik and Sparks 1999; Wylie et al. 1999) may also account for possible changes in eruptive behaviour.

Satisfactory comprehension of the role played by these different processes has not yet been achieved, especially for the non-linear effects of their combinations that are of paramount importance for unravelling the physics of eruptive dynamics. Several studies have been focused on the processes acting within the magma chamber (i.e. magma mixing and fresh magma injection; Eichelberger and Izbekov 2000; Huppert and Woods 2002) and the conduit system (Jaupart and Allegre 1991; Gudmundsson and Philipp 2006; Martel and Poussineau 2007; Preece et al. 2016). Recently, attention has been paid to modifications of the conduit-feeding system geometry able to alter the eruptive (or pre-eruptive) equilibrium (Massaro et al. 2018). The conduit-feeding system connects magma chamber (or reservoir) to the Earth surface, allowing magma to rise. Its structure and dimensions are considered among the most relevant parameters influencing the eruptive behaviour (e.g. Scandone et al. 2007; Melnik et al. 2008; Costa et al. 2009a, 2011; Sulpizio et al. 2016; Massaro 2018).

Several models assumed a simple geometric configuration for the conduit-feeding system described by a cylindrical conduit connected to a deeper chamber (Dobran 1992; Varekamp 1993; Macedonio et al. 1994; Melnik 2000; Macedonio et al. 2005; Colucci et al. 2014). However, geological evidence indicates that volcanic eruptions are mainly fed through dykes (e.g. Eichelberger and Izbekov 2000; Gudmundsson and Brenner 2005; Costa et al. 2009a; Maccaferri et al. 2011; Zellmer and Annen 2014). Likewise, dykes are the only viable mechanism for developing a pathway through the brittle crust from a deep magma chamber to the surface during the initial stages of an eruption (Rubin 1995; Melnik et al. 2008; Rivalta et al. 2015).

A cylindrical conduit may develop only at shallow levels, favoured by erosion of wall rock (Costa et al. 2007a; Melnik et al. 2008; Costa et al. 2009a; Melnik and Costa 2014). In many cases, the arrival of a dyke to the surface does not necessarily result into a continuous feeding of eruptive activity, but the coarse balance of driving and resisting forces may lead the eruptive system close to an equilibrium state (quasi-equilibrium) with formation of lava lakes and domes (Sulpizio et al. 2016). Effusive eruptions may shift to Strombolian and/or Vulcanian explosive phases depending on the interplay between the driving pressure and degassing-dependent viscous forces (Wylie et al. 1999; Ripepe et al. 2013).

The Fuego de Colima volcano (Mexico) exhibited quasi-equilibrium conditions (at least) in the last five centuries (Luhr 2002), developing a summit dome that is occasionally dismantled by Vulcanian and (rarely) sub-Plinian explosive eruptions (e.g. Bretón-González et al. 2002; Gavilanes-Ruiz et al. 2009; Saucedo et al. 2010). The 1913 eruption was the last sub-Plinian event at Fuego de Colima and provides a well-documented example of the eruptive style transition from dome extrusion to a sub-Plinian explosive event (Saucedo et al. 2010). In this work, we present a first-order discussion of the physical processes that drove the transition of the 1913 eruption from a slow dome extrusion into an explosive eruption by means of numerical simulations carried out with the CPIUD code (Condotto PIU Dicco; Costa et al. 2009a, 2011), experimental petrology (Macías et al. 2017) and data from finite element modelling, which provided assessment of the effect of gravitational loading on the volcano spreading (Norini et al. 2010). The CPIUD code is a numerical model that simulates a 2-D steady-state magma flow within conduits having elliptical cross sections, taking into account the wall-rock elasticity and local tectonic stress. Quasi-static elastic deformation of the dyke-shaped conduit is accounted for by an analytical solution (Muskhelishvili 1963), which couples cross-sectional area with the magma pressure. The viscosity of the magma is assumed constant, while dissolved and exsolved gas mass fraction is solved as function of solubility coefficient and exponent (Costa et al. 2009a). The model allows input into the conduit of either liquid magma or pyroclastic particulate, and solves the mass and momentum conservation equations. Input parameters include the depth of magma chamber top (i.e. conduit length), overpressure at the top of the magma chamber, rheological properties of magma (i.e. magma viscosity) and geometry of the conduit feeding system (pure dyke, pure cylinder or deeper dyke passing into a shallower cylinder).

Adopting an approach similar to Massaro et al. (2018), the model was here used to reconstruct the first-order geometry of the conduit-feeding system during the sub-Plinian phase of 1913 eruption, taking into account the volcanological data (Saucedo et al. 2010, 2011; Bonasia et al. 2011) as input and constraints for the numerical simulations. In particular, the mass discharge rate (MDR) estimated for the main explosive

event recorded in the C_1 fall bed, and the lithic-ejecta types within C_1 (Saucedo et al. 2011) were used as target values of the numerical simulations and as constraints for the fragmentation depth, respectively. We assumed hybrid geometrical configuration composed of a deeper dyke connected to a shallower cylindrical conduit, as inferred from geophysical observations (Salzer et al. 2014). The results of numerical simulations were then compared with the available volcanological (Saucedo et al. 2010), geophysical (Spica et al. 2017) and experimental petrology (Macías et al. 2017) data in order to evaluate the possible magmatic (magma chamber overpressure) or non-magmatic (lowering of lithostatic load) triggers of the observed eruptive style transition.

Geological framework

Fuego de Colima volcano is located in the western part of the Trans-Mexican Volcanic Belt, a calc-alkaline continental volcanic arc in the central part of Mexico (Fig. 1a). Together with Nevado de Colima, it constitutes a volcanic complex lying on a basement of Cretaceous limestones and intrusive rocks, covered by a graben-fill sequence including Quaternary alluvial, colluvial and lacustrine deposits, with andesitic volcanic rocks in the upper 2 km. Since the onset of the recorded eruptive activity, the behaviour of Fuego de Colima has been characterized by summit dome growth and intermittent explosive activity that sometimes culminated in large sub-Plinian (and Plinian) eruptions eventually leading to complete destruction of the dome (as in 1585, 1606, 1622, 1818, 1890 and 1913; De la Cruz-Reyna 1993; Luhr 2002). To date, Fuego de Colima is considered the most active volcano in Mexico (De la Cruz-Reyna 1993; Bretón-González et al. 2002; Vargas-Bracamontès et al. 2009) with more than 43 eruptions since 1576 (Luhr and Carmichael 1981; Medina-Martínez 1983; De la Cruz-Reyna 1993; Saucedo et al. 2005). The effusive-to-explosive cyclical nature of its long-term activity was extensively discussed in previous studies (Luhr and Carmichael 1980, 1990; Luhr 2002). The last eruptive cycle started in 1818 and ended with the 1913 sub-Plinian eruption, which is the object of the present study. A remarkable eruptive event occurred in July 2015 when the summit dome was completely dismantled producing pyroclastic density currents (PDCs) that filled the Montegrande and San Antonio ravines along the southern slopes of the volcano (Capra et al. 2016).

The 1913 eruption

The 1913 sub-Plinian eruption occurred nearly a century later the 1818 eruption. This period was characterized by low to moderate intensity eruptive activity. Following historical accounts, the eruptive activity resumed in 1869, 51 years after the 1818 eruption. Between 1869 and 1909, only two lava

effusions occurred, while thousands of low to moderate intensity Vulcanian eruptions punctuated the period (Díaz 1906), peaking in frequency and intensity between 1900 and 1903 (Navarro and Cortés 1993; Bretón-González et al. 2002; Savov et al. 2008).

A series of low-intensity explosions on 17 January heralded the onset of 1913 eruption and partially destroyed the summit dome (Waitz 1915; Ortiz 1944; Bretón-González et al. 2002; Saucedo et al. 2010). During the following 24 h, the eruption progressed through three eruptive phases (Saucedo et al. 2010). The opening Phase (1) was characterized by explosions that produced small Merapi-type block-and-ash flows (units F1, F2, F3; Fig. 1b) and a dilute PDC (unit S1). Phase (2) witnessed strong Vulcanian explosions that produced concentrated PDCs (unit F4) and a dilute PDC (unit S2). This phase cleared the vent and destroyed almost completely the summit dome decompressing the conduit system (Saucedo et al. 2010). The sub-Plinian (climactic) Phase (3) established a ca. 23 km high column that dispersed fallout deposits to the NE (unit C_1 ; Fig. 1b). At the end of Phase (3), the sustained column collapsed, generating dilute PDCs (unit S3) and pumice-rich concentrated PDCs (unit F5) that dispersed radially from the vent up to a distance of 15 km (Saucedo et al. 2010). The 1913 eruption changed the volcano morphology, causing a loss of 100 m in height and developing a 400 m wide and 350 m deep summit crater (Waitz 1915; Bretón-González et al. 2002).

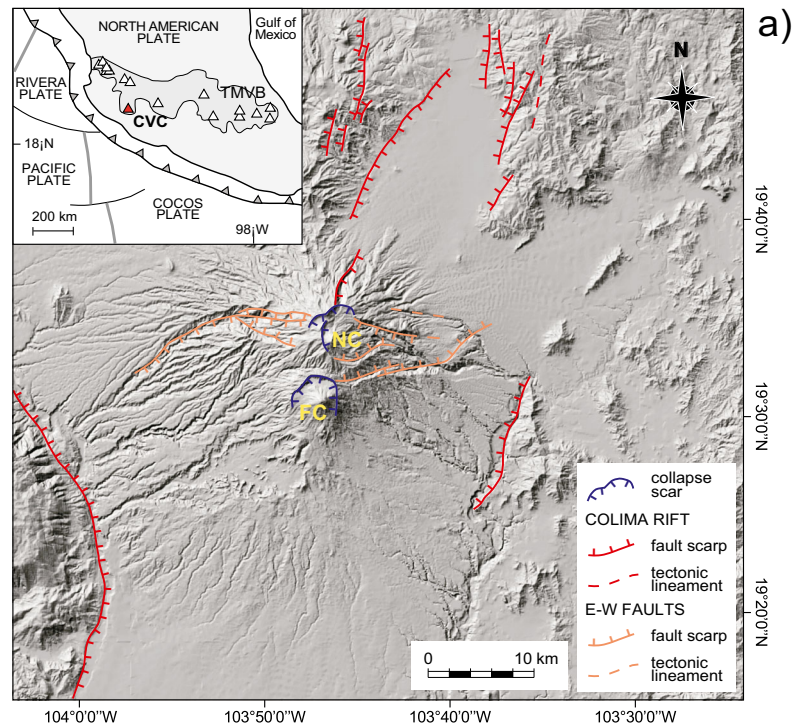
The main fallout deposit of Phase (3) (Fig. 1b) covered an area of ca. 191,000 km², with an estimated volume of ca. 0.56 km³ (ca. 0.23 km³ dense rock equivalent, DRE; Saucedo et al. 2011), representing ca. 80% of the total erupted volume of the eruption. Bonasia et al. (2011) reported a total mass of ca. 2.36×10^{11} kg, a column height of 25 km and a DRE volume of fallout deposits of ca. 0.22 km³, in good agreement with Saucedo et al. (2011), who calculated ca. $2\text{--}6 \times 10^{11}$ kg. Connor et al. (2016) provided a range of the erupted mass between ca. 5.5×10^{10} kg (volume of 0.04–0.06 km³, column height of ca. 14 km) based on field data and ca. 1.4×10^{11} kg (volume of 0.1–0.5 km³) by taking into account the thickness derived from historical accounts. Considering typical uncertainties in tephra volume estimations (Bonadonna and Costa 2012; Bonadonna et al. 2015), the latter values of the erupted mass and volume are in agreement with those of Saucedo et al. (2011) and Bonasia et al. (2011), and will hereafter be used for the purposes of this paper.

Methodology

Numerical modelling

The numerical simulations were carried out using the CPIUD code (Costa et al. 2009a, 2011) in order to obtain a first-order

Fig. 1 a Morphotectonic map of the Colima Volcanic Complex (NC = Nevado de Colima volcano; FC = Fuego de Colima volcano) and Colima Rift with the main tectonic and volcano-tectonic structures (modified from Norini et al. 2010). In the inset, the location of the Colima Volcanic Complex (CVC) within the Trans-Mexican Volcanic Belt (TMVB) is shown in the frame of the subduction-type geodynamic setting of Central America. **b** Schematic stratigraphy (and volcanological interpretation) of the products erupted during the 1913 eruption of Fuego de Colima (modified from Saucedo et al. (2010) and Sulpizio et al. (2015))



reconstruction of the conduit-feeding system during the sub-Plinian fallout phase of the 1913 eruption of Fuego de Colima. This is assumed as a “snapshot” of the climactic phase of the eruption, being the model based on a steady-state solution. The CPIUD code solves a set of cross section averaged equations derived from the generalization of Macedonio et al. (2005) model as proposed by Costa et al. (2009a). We tested a range of hybrid geometrical configurations of the conduit-feeding system, obtained varying the respective lengths of the lower dyke and the shallower cylinder. In CPIUD code, the magma flow in the conduit is governed by mass and momentum balance equations under quasi-steady-state conditions:

$$\frac{\partial}{\partial z}(\rho AV) = 0 \tag{1}$$

$$V \frac{\partial V}{\partial z} = -\frac{1}{\rho} \frac{dP}{dz} - g - ffr \tag{2}$$

where ρ is the magma density, A is the cross-sectional area, V is the mixture velocity, and g is the gravity acceleration. The ffr friction term is expressed below the fragmentation level as (Costa et al. 2007a, 2009a)

$$ffr = 4 \frac{\mu}{\rho} \frac{a^2 + b^2}{a^2 b^2} V \tag{3}$$

where a and b are the major and minor axes of the elliptical cross section, and μ is the effective magma viscosity, here assumed constant. Above fragmentation level, $ffr = 0$. The magma density ρ is defined considering a homogeneous mixture as in Macedonio et al. (2005):

$$\frac{1}{\rho} = \frac{xe}{\rho g} + \frac{1-xe-xc}{\rho l} + \frac{xc}{\rho c} \tag{4}$$

where ρg is the gas density, ρl is the density of the melt phase, ρc is the crystal density, xe is the exsolved gas mass fraction, and xc is the crystal mass fraction. The exsolved and the dissolved gas mass fraction can be expressed as

$$xe = \frac{xtot-xd}{1-xd} (1-xc); \quad xd = s P^n \tag{5}$$

where $xtot$ is the initial total gas mass fraction, xd is the dissolved gas mass fraction, and the solubility exponent n and the constant solubility coefficient s in the solubility law (Battino and Clever 1966) depend on magma composition only. The gas phase (perfect gas) and the condensed phases are compressible.

This model contains some important assumptions, summarized as follows:

1. Cross section averaged variables are used to describe magma flow in the conduit in which vertical deformations are much smaller than horizontal ones.

2. Quasi-static elastic deformation of the conduit is accounted by an analytical solution (Muskhelishvili 1963) that couples the cross-sectional area with the magma pressure.
3. Magma flow in the conduit is approximated as steady state, assuming that the time-scale of pressure variations at the conduit base (hours) is much longer than the travel time of the magma in the conduit (few minutes).
4. Both the gas and the condensed phase (liquid and crystals) are assumed to have the same velocity.
5. As a first-order approach, isothermal assumption is justified by the heat capacity of the magmatic mixture and effective heat transfer between the condensed phase and rapidly expanding gas (Wilson et al. 1980).
6. Following points 3 and 4, magma can enter the conduit in either homogeneous or the bubbly flow regime, and exits in the particulate flow regime, after fragmentation is assumed to occur when the gas volumetric fraction α reaches a critical value α_c (Costa et al. 2009a; Macedonio et al. 2005), corresponding to the bubble maximum packing (typically $\alpha_c \approx 0.75$; Sparks 1978).
7. Magma behaves as a compressible liquid even when the pressure is greater than the bubble nucleation pressure. If the pressure is lower than the nucleation pressure, the gas exsolves and a liquid–gas mixture becomes much more compressible. It is assumed that no supersaturation is required for bubble nucleation.

A fixed pressure is assumed as boundary condition at the base of the dyke because the pressure change is much longer than magma ascent time through the conduit. Pressure at the conduit bottom is fixed, defined as Pch (at magma chamber top), and choked flow conditions are assumed at the conduit exit.

To integrate the governing equations avoiding singularity at the outlet (exit condition) in Eqs. (1) and (2), Costa et al. (2009a) introduced two characteristic velocities, “isothermal” sound velocity in the erupting magma s (Macedonio et al. 2005) and wave velocity in a deformable tube c (Young 1808; Shapiro 1977; Paidoussis 2006):

$$\frac{1}{s^2} \equiv \left(\frac{d\rho}{dP} \right)_T \quad \text{and} \quad \frac{1}{c^2} \equiv \left(\frac{\rho dA}{AdP} \right)_T \tag{6}$$

where T is the temperature of the gas phase. Considering these velocities in mathematical manipulations, the governing Eqs. (1) and (2) can be rewritten using the Mach number $M = V/s$ as independent variable. Consequently, the new equations are integrated between the initial Mach number at the conduit inlet, Mi , and the Mach number at the conduit exit, Mo , which is set equal to $Mo = 1/(1 + \gamma^2)^{1/2}$ (with $\gamma = s/c$), defining the choked flow condition. For simplicity, we fix the conduit length L (instead of the Mach number) at the conduit entrance; therefore, the value of Mi is searched using the standard

shooting methods, until the mathematical integration gives $z = L$ at the conduit exit, where $M = M_0$ (Costa et al. 2009a).

The dimensions of the major and minor semi-axes (a and b) of the dyke depend on the magmatic overpressure ΔP (Muskhelishvili 1963; Mériaux and Jaupart 1995; Costa et al. 2007a), which is in turn considered as the difference between the local magmatic pressure and lithostatic pressure:

$$a(z) = a_0(z) + \frac{\Delta P}{2G} [2(1-\nu)b_0(z) - (1-2\nu)a_0(z)] \quad (7)$$

$$b(z) = b_0(z) + \frac{\Delta P}{2G} [2(1-\nu)a_0(z) - (1-2\nu)b_0(z)] \quad (8)$$

where G is the rigidity of wall-rock and ν is the Poisson ratio. The a_0 and b_0 are the initial unpressurized values of the dyke semi-axes. Equations (7) and (8) are based on the assumption that elastic deformation can be locally described as plain strain approximation (Muskhelishvili 1963). This implies that these relationships can be applied only if the local length-scales characterizing vertical changes in the conduit geometry and fluid pressure are much larger than the transversal dimensions of the conduit (i.e. the conduit diameter D or the dyke thickness H). Moreover, Eqs. (7) and (8) are not valid near the free surface where both boundary and topographic effects can be important. Purely elastic rock properties are assumed, and no rock failure is allowed. This latter assumption can be assessed a posteriori if solutions are likely to exceed the wall-rock strength. The transition from dyke to cylinder is a parameterised value (Costa et al. 2009a); LT and wT define the position and the vertical extent of the transition zone, approximating the behaviour of a dyke in the limit $a \gg b$ and recover the case of a cylinder when $a = b = R$. It is worth noting that in this model, the magma properties are treated in an approximate way. This includes equilibrium water exsolution, absence of gas overpressure with respect to magma pressure and constant viscosity assumption.

Input data and constraints

Input values for the model are obtained from geophysical, petrological, rock property, and stratigraphic data of the 1913 eruption collected from the literature (Touloukian et al. 1989; Atlas et al. 2006; Savov et al. 2008; Costa et al. 2009a; Saucedo et al. 2010; Bonasia et al. 2011; Alvarez and Yutzis 2015; Connor et al. 2016; Macias et al. 2017), and are summarized in Table 1. Seismic tomography data indicate that the feeding system of Fuego de Colima is composed of two magma chambers at different depths (Spica et al. 2017). The shallow reservoir has its top at depth of ca. 6 km within Cretaceous limestones (Norini et al. 2010) and has an estimated volume of ca. 40 km³ (Cabrera-Gutiérrez and Espindola 2010). The deep reservoir has its top at depth of ca. 15 km, and a volume > 650 km³ (Spica et al. 2017). The deep reservoir supplies

magma into the shallow magma chamber, as demonstrated by petrological studies indicating periodical arrival of magma batches triggering mixing and mingling processes with the resident magma (Macias et al. 2017). Due to the small erupted volume during the 1913 eruption, we assume that the eruptive dynamics of the climactic phase was controlled by the shallower part of the feeding system. This is because the erupted magma volume (ca. 0.22 km³; Bonasia et al. 2011) is significantly lower than the estimated volume of the shallower magma chamber (ca. 40 km³; Cabrera-Gutiérrez and Espindola 2010). The total length of the conduit connecting the shallow magma chamber to the surface was set at ca. 6 km, as suggested by the mineral phase equilibria (presence of fresh amphibole crystals, which are stable at 170–210 MPa; Luhr 2002; Macias et al. 2017), melt inclusions (Reubi and Blundy 2008) and tomographic data (Núñez-Cornù et al. 1994; Medina-Martinez 1983; Zobin et al. 2002; Zamora-Camacho et al. 2007; Alvarez and Yutzis, 2015).

The CPIUD simulations were carried out considering a reference value of magma overpressure (i.e. the pressure driving the eruption) of 20 MPa at the top of the magma chamber, although other values were also tested. Such a reference value is sufficient for driving explosive eruptions from a magma chamber at 6 km of depth (Costa et al. 2011) and is also in the range of overpressure assessed for Colima magmas through rapid decompression experiments (Lavallè et al. 2012). It is important to note that changing the overpressure in a reasonable range of values (10–60 MPa) does not influence the model outputs significantly and, in particular, the calculated MDRs are of the same order of magnitude (Massaro 2018).

Magma temperature was set at 950 °C, as suggested by petrological experiments of Savov et al. (2008) carried out using the andesitic melt composition of the 1913 eruption and the presence of amphibole crystals. The pre-eruptive concentration of dissolved water in the melt was assessed based on ion-probe studies of melt inclusions trapped in pyroxenes of the 1913 eruption magmas. Luhr et al. (2006) reported H₂O contents between 5.7 and 6.2 wt%, while Atlas et al. (2006) provided a lower value of 3.4 wt%. Because the 1913 products contain stable hornblende crystals (stable in silicate melts containing 3–4% of H₂O; Rutherford and Hill 1993; Moore and Carmichael 1998; Carmichael 2002; Savov et al. 2008), we considered the value of Atlas et al. (2006) for calculating the effective melt viscosity of the 1913 eruption.

The melt viscosity of the 1913 magma was calculated using the Giordano et al. (2008) model. For estimating magma viscosity (Costa et al. 2009b; Cimarelli et al. 2011), we accounted for a crystal mass fraction of about 10%, as assessed from the petrography of 1913 erupted products (Savov et al. 2008; Massaro 2018). The effect due to the presence of bubbles on magma rheology was neglected. An effective mean viscosity value of the order of 10⁵ Pa s⁻¹ was estimated. The choice of using an effective mean viscosity value rather than more

Table 1 Parameters used in the CPIUD simulations

Notation	Description	Value	References
x_{tot}	Concentration of dissolved gas (wt%)	3.4	Atlas et al. 2006
x_c	Crystal fraction (wt%)	0.10	Massaro 2018
L	Conduit length (m)	6000	Macias et al. 2017
ρ_l	Density of the melt phase (kg m^{-3})	2550	Bonasia et al. 2011
ρ_c	Density of the crystal (kg m^{-3})	2650	Bonasia et al. 2011
ρ_r	Host rock density (kg m^{-3})	2800	Touloukian 1989
T	Magma temperature (K)	1223	Savov et al. 2008
μ	Effective Magma viscosity (Pa s^{-1})	10^5	Giordano et al. 2008
P_{ch}	Magma chamber pressure (MPa)	180–160	Macias et al. 2017
s	Solubility coefficient ($\text{Pa}^{-1/2}$)	4.1×10^{-6}	Costa et al. 2009a
n	Solubility exponent	0.5	Costa et al. 2009a
G	Static host rock rigidity (GPa)	13	Touloukian 1989
ν	Poisson ratio	0.3	Touloukian 1989
β	Bulk modulus of melt/crystal (GPa)	10	Costa et al. 2009a
Conduit geometry parameters			
L	Magma chamber depth	6000 m	Macias et al. 2017
L_T	Transition depth (range)	500 m	This work
w_T	Transition width length	200 m	This work
W	Width of dyke (range)	200–2000 m	This work
H	Thickness of dyke (range)	10–40 m	This work
D	Conduit diameter	10–40 m	This work

sophisticated viscosity models is adequate as CPIUD considers cross section averaged variables. Moreover, the model does not account for magma temperature variations, and gas overpressure with respect to magma pressure (Costa et al. 2009a). A more realistic description of the magma viscosity should account for the coupling with dissolved water, magma cooling with country rocks, viscous dissipation, crystal resorption and intrinsically two-dimensional effects (e.g. Costa and Macedonio 2005; Costa et al. 2007c; Cimarelli et al. 2011). All these effects can change the local magma viscosity of an order of magnitude (Costa et al. 2007b, c; Cimarelli et al. 2011).

The static rigidity of Cretaceous limestones hosting the shallow magma chamber was assessed at 13 GPa (Touloukian et al. 1989; Table 1). The adopted geometric configuration for the conduit-feeding system of the 1913 eruption is a dyke connected to the uppermost magma chamber that evolves into a cylindrical conduit at shallow depths, which is suggested as the most stable geometry configuration for volcanic conduits reaching the surface (Costa et al. 2009a; Rivalta et al. 2015). The constraints and target values for the CPIUD simulations derive from volcanological and subsurface data for the 1913 erupted products (Norini et al. 2010; Saucedo et al. 2010, 2011; Bonasia et al. 2011; Table 2), to reduce the uncertainty of the model inversion as much as possible.

The exclusive occurrence of lava lithic fragments in the main C_1 fallout deposit (Saucedo et al. 2010) indicates that

the fragmentation level was shallower than ca. 2 km during the climactic Phase 3, in agreement with the reconstructed subsurface stratigraphy (Norini et al. 2010). Thus, we assume that lithic erosion mainly occurred at or above the fragmentation depth (Barberi et al. 1989; Macedonio et al. 1994; Costa et al. 2009a; Campbell et al. 2013). The mass discharge rate (MDR) represents the main target value of the CPIUD model outputs. A peak MDR of $8.9 \times 10^7 \text{ kg s}^{-1}$ was obtained using the Mastin et al. (2009) empirical relationship considering a maximum column height of 25 km (as estimated by Bonasia et al. 2011). A mean MDR equal to $2 \times 10^7 \text{ kg s}^{-1}$ was calculated by taking into account the total erupted mass of ca. $2.36 \times 10^{11} \text{ kg}$ from Bonasia et al. (2011) and a time duration of ca. 3.5 h for the sustained column phase of the 1913 eruption (from 11:30 a.m. to ca. 15:00 p.m. local time; Saucedo et al. 2010).

Results

The CPIUD results are shown in Fig. 2, by plotting MDRs versus fragmentation levels. The simulations were carried out using the (initial) width (W) and thickness (H) of the dyke and transition level (TL) between the dyke and the cylindrical conduit as independent input variables, while MDR and fragmentation level are the outputs. It is important to stress that the solutions of the conduit-feeding system geometry are non-unique (e.g. Anderson and Segall 2011, 2013; Costa et al.

Table 2 Constraints used for the CPIUD simulations. Volume (V , from Bonasia et al. 2011), mass discharge rate (MDR, calculated with Mastin et al. 2009 equation, using the value reported in Bonasia et al. 2011), and fragmentation level (FL, from Norini et al. 2010)

Notation	Description	Value	References
V	Total erupted volume DRE (km^3)	0.22	Bonasia et al. (2011)
MDR	Mass discharge rate, peak value (kg s^{-1})	8.9×10^7	Mastin et al. (2009)
MDR_m	Mass discharge rate, mean value (kg s^{-1})	ca. 2×10^7	Mastin et al. (2009)
FL	Fragmentation level (m)	< 2000	Norini et al. (2010)

2009a; Massaro et al. 2018) but represent the best compromise between the volcanological data and the controlling physical parameters of the model (Costa et al. 2009a). The best match solutions were chosen by comparing the CPIUD outputs versus the target range of MDR and the maximum depth of lithic provenance (ca. 2 km). The target value of the peak MDR is $8.9 \times 10^7 \text{ kg s}^{-1}$ (Bonasia et al. 2011), which is similar to that

reported by Saucedo et al. (2011) and to the maximum estimate provided by Connor et al. (2016) taking into account historical data. The mean MDR value obtained from the erupted mass (from Bonasia et al. 2011) and time duration (from Saucedo et al. 2010) were used as a lower limit of the acceptable output values (Fig. 2). Dyke width W between 200 and 5000 m and dyke thickness H from 10 to 80 m were

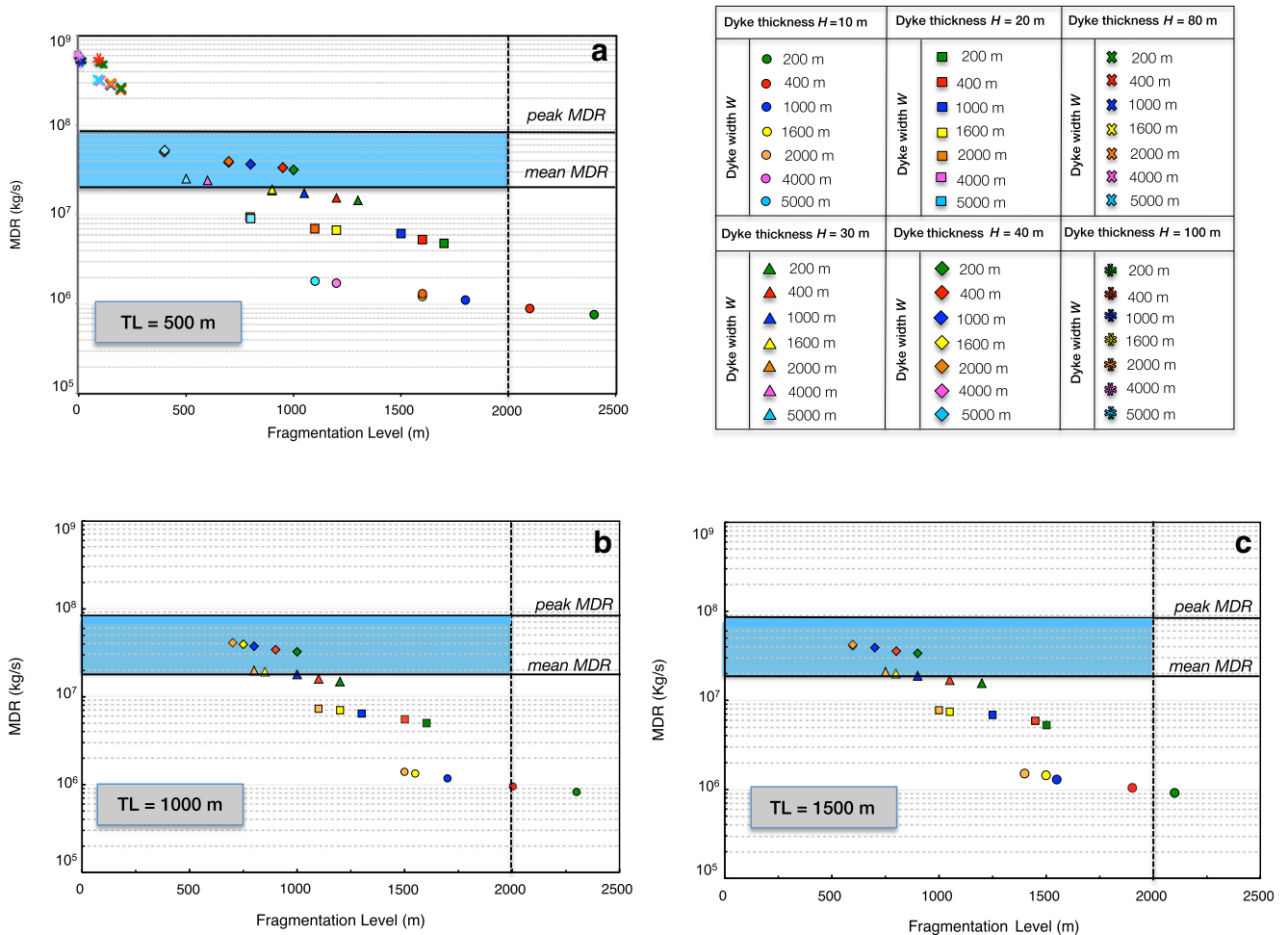


Fig. 2 Outputs of the CPIUD simulations for the sustained explosive phase of 1913 eruption. The diagrams show the variation of MDR versus fragmentation level for a conduit/feeding system composed of an elongated dyke passing into a cylinder conduit near the surface. The simulations are carried out with dyke width W from 200 to 5000 m and dyke thickness H from 10 to 100 m, considering three dyke-to-conduit

transition levels at 500 (a), 1000 (b), and 1500 m (c). The whole set of simulations is shown only for $TL = 500$ m. The blue area corresponds to the acceptable range of MDRs between the mean and maximum values obtained from Bonasia et al. (2011) and Saucedo et al. (2010), respectively

explored (Table 1). For simplicity, the diameter of the cylindrical conduit (D) was fixed equal to the dyke thickness H .

Different model runs were performed considering a transition level (TL) between the dyke and the cylinder conduit at depths of 500, 1000 and 1500 m. Results show that the depth variation does not influence significantly the model outputs (Fig. 2). We assumed TL equal to 500 m on the basis of InSAR data indicating the present-day pressure source around that depth (Salzer et al. 2014).

A slight deepening of the fragmentation level is observed increasing dyke width W and decreasing thickness H . At the same time, a sharp decrease of MDR occurs decreasing dyke thickness H . Figure 2 shows that the best fit solutions of the model are for dyke having thickness H of about 40 m and a width W ranging from 200 to 5000 m. Possible solutions are also obtained for thickness H of 30 m and a width W ranging from 2000 to 5000 m. These results give a first-order geometrical configuration of the conduit/feeding system of Fuego de Colima volcano during the 1913 eruption. The best-fit geometric configurations correspond to dyke volumes in the range of 3.45×10^7 to 3.45×10^8 m³, as reported in Table 3.

Discussion

Geometry of the conduit-feeding system before the sub-Plinian explosive phase

Massaro (2018) reconstructed the geometric configuration of the conduit-feeding system of Fuego de Colima during the 1998–2015 period of (mainly) dome extrusion and lava flows using the magma flow model of Costa et al. (2007a) and Melnik and Costa (2014), who generalized the model proposed by Melnik and Sparks (2005) for a shallow dyke to cylinder conduit and a dual magma chamber system. The model accounts for rheological changes due to volatile loss and temperature-driven crystallization. The best fit geometry for lava dome eruptions is described by a deep dyke having width W of 200 m and thickness H of 40 m passing into a 500-m long cylindrical conduit at shallow depths (Fig. 3a). We

Table 3 Volumes of hybrid geometries obtained with CPIUD simulations, for a fixed dyke thickness $H=40$ m and transition level $TL=500$ m. The total erupted volume DRE is equal to 2.2×10^8 m³ (from Bonasia et al. 2011)

Dyke width W	Volumes
200 m	3.45×10^7 (m ³)
400 m	6.91×10^7 (m ³)
1000 m	1.73×10^8 (m ³)
1600 m	2.76×10^8 (m ³)
2000 m	3.45×10^8 (m ³)

assume a similar geometry also for the conduit-feeding system during the time period preceding the 1913 eruption, considering similar conditions of dome extrusion and magma compositions. This assumption is also supported by the combination of estimated magma volumes of the 1913 sub-Plinian explosive phase combined with petrography of the erupted products. The products erupted after 1913 or in the period between 1818 and 1913 not contain hornblende, or, when present, it shows reaction borders indicating prolonged ascent times at pressures below 170–210 MPa (6–7 km of depth, Macias et al. 2017). In other words, these products underwent long transit times in the conduit system of Fuego de Colima before eruption, as typical of dome or low effusion rate lava flow eruptions (e.g. Luhr and Carmichael 1980; Mora et al. 2002; Macias et al. 2017). The presence of fresh hornblende in the 1913 magma indicates the rapid withdrawal of magma from the shallow magma chamber, located at 6 km of depth and therefore within the stability field of amphibole. The volume stored in the conduit system of 1913 was less than the total erupted of ca. 220×10^6 m³ estimated by Bonasia et al. (2011). This allows us to constraint the possible geometrical configurations obtained by CPIUD simulations, excluding volumes of the conduit-feeding system greater or comparable to the erupted volumes (see Table 3). As such, geometrical configurations with dyke width W equal to 1600 m (corresponding to volume of 276×10^6 m³) can be excluded, and the solutions with W equal to 1000 m (volume of 173×10^6 m³) are less probable. Consequently, dyke widths equal to 200 and 400 m are considered more likely. This leads to a refinement of the geometrical configuration of the conduit-feeding system before the sustained phase of 1913 eruption with an elongated dyke, having width W of 200–400 m and thickness H of 40 m, which evolves at shallow depths into a cylindrical conduit with a diameter D of 40 m and a length of 500 m.

What triggered the sub-Plinian explosive phase?

We consider Fuego de Colima during dome extrusion before the 1913 eruption as an open conduit system close to equilibrium, and the driving pressure, given by the magma chamber overpressure (P_0) minus the pressure required for maintaining open the dyke (ΔP_{0m}), is balanced by the weight of magma column (i.e. magmastatic loading, ρgh), the lithostatic stress (σ_l) and the resisting forces per unit area (R_p ; Jaupart and Allegre 1991; Gudmundsson 2012; Sulpizio and Massaro 2017):

$$P_0 - \Delta P_{0m} = \rho gh + \sigma_l + R_p \quad (9)$$

Being the conduit open and dome extrusion in process, the main variables that can abruptly change to alter the equilibrium and trigger a transition to the explosive phase of 1913 eruption are P_0 (magma overpressure) and σ_l (component of the

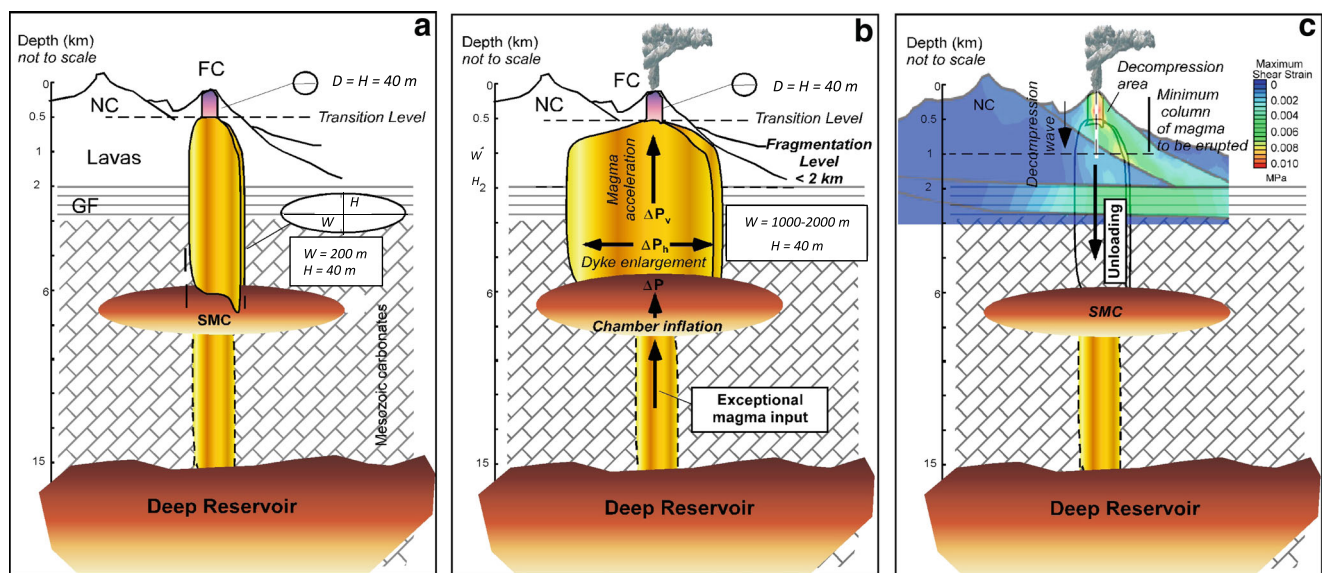


Fig. 3 Cartoon showing the main geometrical changes of the conduit-feeding system of Fuego de Colima during the effusive-to-explosive transition of the 1913 eruption (not to scale). NC Nevado de Colima, FC Fuego de Colima, GF Graben filling deposits; SMC shallow magma chamber. **a** Geometrical configuration of the conduit/feeding system prior to the 1913 eruption. The deep reservoir has its top at depth of ca. 15 km of depth and is weakly connected to the shallower magma chamber with its top at depth of ca. 6 km. This latter is connected to the surface by a dyke (width $W = 200$ m, thickness $H = 40$ m) that evolves into an upper cylindrical conduit at depth of 500 m (transition level TL). The diameter

of the cylinder D is equal to the dyke thickness H . **b** Diagram of the variation of magma overpressure (ΔP) as function of the volume of magma injected into a magma chamber (ΔV) immersed in a perfect elastic medium for different magma chamber volumes. The red dashed line indicates a $\Delta P = 25$ MPa. **c** Geometrical configuration of the volcanic system of Fuego de Colima showing the possible effects of a lowering of the lithostatic load in the upper part of the conduit induced by a sector collapse of sudden lateral spreading. The location and magnitude of the maximum strain rate affecting the summit volcano are shown as derived from numerical simulations of Norini et al. (2010)

lithostatic stress). An effusive-to-explosive transition in eruptive style can be triggered by an increase in magma overpressure (magmatic triggering), a decrease of lithostatic pressure (non-magmatic trigger), a decrease of the resisting forces due to non-linear effects (e.g. Woods and Koyaguchi 1994; Melnik and Sparks 1999; Voight et al. 2006), or a combination of them.

The historical activity at Fuego de Colima indicates that sustained (sub-Plinian) explosive eruptions as 1913 are rare (one about every 100–200 years), and the eruptive behaviour is dominated by long periods of dome extrusion occasionally interrupted by small Vulcanian explosive eruptions (Luhr and Carmichael 1980; De la Cruz-Reyna 1993; Luhr 2002; Gavilanes-Ruiz et al. 2009; Lavallè et al. 2012). This means that either magmatic or non-magmatic processes able to alter the usual eruptive dynamics and trigger a sustained explosive eruption occur occasionally.

The most common way to increase magma overpressure and trigger an explosive eruption is the arrival of fresh magma into a shallow magma chamber (e.g. Eichelberger and Izbekov 2000; Smith et al. 2004; Sigmarsson et al. 2011). Mineralogical and geochemical data of the 1913 juvenile products (banded scoriae, plagioclase and pyroxene phenocrysts with reaction rims) show evidence of magma mixing well before the sustained (sub-Plinian) explosive phase (Luhr and Carmichael 1980; Savov et al. 2008; Saucedo et al. 2010; Macias et al. 2017), suggesting that the injection of fresh

magma into the shallow magma chamber occurred frequently. Crummy et al. (2014) found that pulses of phlogopite-rich mafic magmas periodically enter the Colima plumbing system on timescales of a few thousand years. This is in agreement with the results of Macias et al. (2017), who highlighted how the 1818 and 1913 magmas are the products of mixing of andesitic resident magma with mafic pargasite-rich batches at a pressure of 170–210 MPa. The repeated injection of fresh magma into the shallow chamber accounts for observed disequilibrium textures in 1913 phenocrysts and compositional variability in minerals and groundmass (Macias et al. 2017) or pattern in trace elements (Savov et al. 2008). This also suggests homogeneous (andesitic) bulk composition of the magma in the shallow magma chamber, with limited difference in temperature between the residing and injected magma (Macias et al. 2017).

Considering a perfectly elastic medium, we can calculate the overpressure induced by injection of fresh magma into the shallower magma chamber (Rivalta et al. 2015). Supposing that magma is supplied in the shallow magma chamber at a rate greater than the effusion rate, magma accumulates in the chamber with time, and this increases the chamber overpressure as

$$\Delta P = \frac{\Delta V}{V} \frac{1}{(\beta_c + \beta_m)} \quad (10)$$

where ΔV is the volume of injected magma, V is the original volume of the magma chamber, β_c is the magma chamber compressibility and β_m is the magma compressibility controlled mainly by bubbles. Both parameters can vary by an order of magnitude, depending on chamber size and depth (Melnik and Sparks 2005). In particular, the magma chamber compressibility depends on the shape of the chamber and on the rigidity of the host medium μ (e.g. Melnik and Sparks 2005; Amoroso and Crescentini 2009; Rivalta 2010). For spherical chambers and $\mu = 3\text{--}25$ GPa, $\beta_c = 0.3\text{--}3$ GPa⁻¹. Magma compressibility β_m is very small for a bubble-free magma (0.04–0.2 GPa⁻¹, Spera 2000) but relatively large if volatiles exsolve (for basaltic magma up to 10 GPa⁻¹ depending on depth; Rivalta and Segall 2008; Rivalta 2010). If we use the minimum value of β_c (0.3 GPa⁻¹) and considering injection of gas-free magma ($\beta_m = 0.04\text{--}0.2$ GPa⁻¹), an injection of ca. $200\text{--}250 \times 10^6$ m³ of magma induces an overpressure of ca. 25 MPa. It is worth note that the volume of injected magma to induce 25 MPa of overpressure may lower of one order of magnitude (to ca. 10×10^6 m³) if the upper values of β_c (3 GPa⁻¹) and β_m (10 GPa⁻¹) are used (i.e. the magma has high volatile content). An increase in magma chamber overpressure would result into growing dyke dimensions (Fig. 3b), because of the partition of overpressure into vertical driving pressure (allowing magma ascent) and horizontal driving pressure (producing rock fracture and enlargement of the dyke). Considering an initial dyke width W of 200 m, the best solutions of CPIUD simulations allow the possibility of dyke enlargement to 2000 m (Fig. 2).

Another argued possibility for triggering the effusive-to-explosive transition during the 1913 eruption is a rapid decompression of the conduit-feeding system (or part of it). Lowering of the lithostatic stress was long claimed as play a fundamental role in triggering volcanic eruptions and in controlling their dynamics (Gudmundsson and Phillip 2006; Andrew and Gudmundsson 2007; Watt et al. 2009; Plateaux et al. 2014; Sulpizio and Massaro 2017). Changes of stress acting on both edifices and magma chambers can be usually related to processes with different characteristic time-scales. In particular, the occurrence of tectonic earthquakes (Walter and Amelung 2007) and sector or flank collapses (Pinel and Jaupart 2005) are short-term processes that can affect eruptive style transition (Sulpizio and Massaro 2017). Concerning earthquakes, no large seismic activity has been reported in the Fuego de Colima area prior to the onset of the eruption in January 1913. There was an earthquake 2 months before (on November 1912) in the region of Acambay graben (Urbina and Camacho 1913), about 400 km from Fuego de Colima. This was the most severe historical earthquake recorded in the area, with a surface magnitude (M_s) of 6.9 (Abe 1981; Suter et al. 1995), but it is hard to infer if it could have had an influence in triggering the 1913 explosive eruption. For example, larger earthquakes struck the area near the

town of Manzanillo (moment magnitude $M_w = 7.6$) in 1995 (García-Pérez and Urrutia-Fucugauchi 1997) or in Tecoman (moment magnitude $M_w = 7.8$) in 2003 (Yagi et al. 2004). In particular, the Manzanillo earthquake occurred at about 90 km from Fuego de Colima, without conditioning volcanic activity, characterized by open conduit system conditions similar to those of 1913.

Sudden explosive eruptions are frequently triggered by a sector or flank collapse unloading the conduit-feeding system (i.e. Mt. St. Helens in 1980, Belousov et al. 2007; Reid et al. 2010; Walter 2011). This most likely occurred in the past at Fuego de Colima (Cortes et al. 2010; Roverato et al. 2011). Particularly, the unloading induced by a collapse was responsible for the explosive eruption of 10–11 July 2015, in which the failure of part of the summit crater produced PDCs with a total volume of 4.5×10^6 m³ (Capra et al. 2016). However, no major sector/flank collapses or summit crater failures have been reported prior to the 1913 eruption at Fuego de Colima.

Another mechanism accounting for reduction in the lithostatic load acting on a volcano is the lateral spreading, defined as the lateral deformation of a volcanic edifice along a basal ductile layer that deforms under the volcano weight (e.g. Lundgren et al. 2004; Norini and Acocella 2011; Acocella et al. 2016). This process was assumed as a trigger for eruptions at different volcanoes around the world (e.g. Etna, Kīlauea, and Piton de la Fournaise; Acocella et al. 2003; Neri et al. 2004; Poland et al. 2017). In our case study, geological/structural data and numerical modelling (Norini et al. 2010; Alvarez and Yutsis 2015) reported a southward (lateral) gravitational spreading of the whole Colima volcanic complex (comprising the Fuego de Colima and Nevado de Colima volcanoes) over the sedimentary fill of the Colima Rift. In particular, published time independent finite element modelling (Norini et al. 2010) highlighted that, beside a general spreading of the volcanic complex, the Fuego de Colima shows shear strain in the order of 8–10 kPa and a vertical displacement up to 16 m in the upper part of the cone (Fig. 3c). These results indicate the susceptibility of Fuego de Colima to southward lateral movement. Being the shear strain and vertical displacement located in the upper part of the Fuego del Colima cone (Fig. 3c), it can be argued that the southward lateral movement occurs as sudden and stepwise rock faulting and brittle deformation (Norini et al. 2010; Alvarez and Yutsis 2015). This mechanism has the same effect that producing a small overpressure in the system, which can alter the MDR. If the value of MDR exceeds a threshold limit, it triggers a transition to an explosive eruption (Woods and Koyaguchi 1994). The explosive activity is maintained as long as the overpressure is balanced and the value of MDR falls below the threshold, restoring effusive eruption conditions (Woods and Koyaguchi 1994).

The eruption of magma contained in the upper part of the conduit could have also a feedback reducing the static load on

the magma chamber. Assuming a magma density of 2100–2500 kg m⁻³ (compatible with the andesitic rock compositions; Luhr 2002), it is necessary to empty 1000–1200 m of the upper conduit in order to have a decompression of 25 MPa, which is in the range hypothesized for the magma chamber overpressure from magma influx. This hypothesis is compatible with the CPIUD results ($W=200$ m, $H=40$ m, $D=40$ m, $TL=500$ m), and the geometric configuration of the conduit/feeding system might remain unaltered passing from dome extrusion to the sub-Plinian explosive phase.

Distinguishing between an internal (magma overpressure) or external (sector/flank collapse and spreading) trigger for the onset of the sub-Plinian explosive phase of 1913 eruption is not straightforward due to the lack of compelling petrological and geophysical evidence. Considering that sub-Plinian (to Plinian) explosive phases are rare compared with effusive activity (dome extrusion and lava flows), it can be argued that the triggers of these sustained explosive eruptions are exceptional events, and the concurrence of more than one has also to be taken into account. Further research and high-quality petrological and geophysical (i.e. deformation) data are thus required to shed light on processes responsible for abrupt changes in eruptive style at Fuego de Colima.

Conclusions

The mechanisms triggering the effusive-to-explosive style transition at the onset of the 1913 eruption of Fuego de Colima were investigated by coupling CPIUD numerical simulations with geophysical, petrological and volcanological data from the literature and hystorical accounts. The best-fit geometry of the conduit-feeding system is that with a dyke width W of ca. 200–400 m and H thickness of ca. 40 m, evolving into a shallower cylindrical conduit with a diameter D of 40 m at depth of 500 m. This geometrical configuration was inferred considering the peak and mean mass discharge rates, with a fragmentation level shallower than 2 km. The results of the numerical simulations do not allow discrimination between a magmatic (magma chamber overpressure) or non-magmatic (lowering of the lithostatic load) trigger for the transition to the explosive phase of the 1913 eruption. A trigger due to magma overpressure would imply enlargement of the dyke during the sustained explosive phase, which is reasonable considering the best-fit results of dyke width W up to 2000 m. On the other hand, an external trigger, such as a lateral spreading of the volcano, would decompress the magma stored in the conduit-feeding system (or the shallow magma reservoir) without requiring a change in dyke dimensions. The calculations show that a lowering of magmastatic pressure of 25 MPa is necessary to induce the eruption of ca. 1000 m of the magma stored in the conduit, which is not so different from the 700–800-m column of magma assumed to

have erupted during the July 2015 eruption. We highlight here that a sudden jerk of volcanic (lateral) spreading of the volcano could trigger cascading processes with non-linear effects on the quasi-equilibrium eruptive state at Fuego de Colima, eventually triggering large explosive eruptions.

Acknowledgements We wish to thank the Editor A. Harris, the Associate Editor R. Cioni and two anonymous reviewers for the suggestions that improved the manuscript.

References

- Abe K (1981) Magnitudes of large shallow earthquakes from 1904 to 1980. *Phys Earth Planet Inter* 27(1):72–92
- Accocella V, Behncke B, Neri M, D'Amico S (2003) Link between major flank slip and 2002–2003 eruption at Mt. Etna (Italy). *Geophys Res Lett* 30(24)
- Accocella V, Neri M, Behncke B, Bonforte A, Del Negro C, Ganci G (2016) Why does a mature volcano need new vents? The case of the new southeast crater at Etna. *Front Earth Sci* 4:67
- Alvarez R, Yutsis V (2015) Southward migration of magmatic activity in the Colima volcanic complex, Mexico: an ongoing process. *Intern J Geosc* 6:1077–1099
- Amoruso A, Crescentini L (2009) Shape and volume change of pressurized ellipsoidal cavities from deformation and seismic data. *J Geophys Res* 114:B02210
- Anderson K, Segall P (2011) Physics-based models of ground deformation and extrusion rate at effusively erupting volcanoes. *J Geophys Res* 116(B7)
- Anderson K, Segall P (2013) Bayesian inversion of data from effusive volcanic eruptions using physics-based models: application to Mount St. Helens 2004–2008. *J Geophys Res* 118(B5):2017–2037
- Andrew REB, Gudmundsson A (2007) Distribution, structure, and formation of Holocene lava shields in Iceland. *J Volcanol Geotherm Res* 168:137–154
- Atlas ZD, Dixon JE, Sen G, Finny M, Martin Del Pozzo AL (2006) Melt inclusions from Volcán Popocatepetl and Volcán de Colima, Mexico: melt evolution due to vapor-saturated crystallization during ascent. *J Volcanol Geotherm Res* 153:221–240
- Barberi F, Cioni R, Santacroce R, Sbrana A, Vecci R (1989) Magmatic and phreatomagmatic phases in explosive eruptions of Vesuvius as deduced by grain-size and component analysis of the pyroclastic deposits. *J Volcanol Geotherm Res* 38:287–307
- Battino R, Clever HL (1966) The solubility of gases in liquids. *Chem Rev* 66(4):395–463
- Belousov A, Voight B, Belousova M (2007) Directed blasts and blast-generated pyroclastic density currents: a comparison of the Bezymianny 1956, Mount St Helens 1980, and Soufrière Hills, Montserrat 1997 eruptions and deposits. *Bull Volcanol* 69(7):701–740
- Bonadonna C, Costa A (2012) Estimating the volume of tephra deposits: a new simple strategy. *Geology* 40:415–418. <https://doi.org/10.1130/G32769.1>
- Bonadonna C, Biass S, Costa A (2015) Physical characterization of explosive volcanic eruptions based on tephra deposits: propagation of uncertainties and sensitivity analysis. *J Volcanol Geotherm Res* 296: 80–100
- Bonasia R, Capra L, Costa A, Macedonio G, Saucedo R (2011) Tephra fallout hazard assessment for a Plinian eruption scenario at Volcan de Colima. *J Volcanol Geotherm Res* 203:12–22

- Brèton-Gonzalez M, Ramirez JJ, Navarro C (2002) Summary of the historical eruptive activity of Volcan de Colima, Mexico 1519–2000. *J Volcanol Geotherm Res* 117:21–46
- Cabrera-Gutiérrez R, Espíndola JM (2010) The 1998–1999 eruption of Volcán de Colima, Mexico: an application of Maeda's viscoelastic model. *Geofis Int* 49(2):83–96
- Campbell ME, Russell J, Porritt LA (2013) Thermomechanical milling of accessory lithics in volcanic conduits. *Earth Planet Sci Lett* 377–378: 276–286
- Carmichael ISE (2002) The andesite aqueduct: perspectives on the evolution of intermediate magmatism in west-central (105–99°W) Mexico. *Contributions Mineral Petrol* 143:641–663
- Cimarelli C, Costa A, Mueller S, Mader HM (2011) Rheology of magmas with bimodal crystal size and shape distributions: insights from analog experiments. *Geochem Geophys Geosyst* 12(7):G07024. <https://doi.org/10.1029/2011GC003606>
- Capra L, Macías JL, Cortés A, Dávila N, Saucedo R, Osorio-Ocampo S, Arce JL, Galvilanes-Ruiz JC, Corona-Cávez P, García-Sánchez L, Sosa-Ceballos G, Vasquez R (2016) Preliminary report on the July 10–11, 2015 eruption at Volcán de Colima: pyroclastic density currents with exceptional runouts and volume. *J Volcanol Geotherm Res* 310:39–49
- Crummy JM, Savov IP, Navarro-Ochoa C, Morgan D, Wilson M (2014) High-K mafic Plinian eruptions of Volcan de Colima, Mexico. *J Petrol* 55(11):2155–2192
- Colucci S, de' Michieli Vitturi M, Neri A, Palladino DM (2014) An integrated model of magma chamber, conduit and column for the analysis of sustained explosive eruptions. *Earth Planet Sci Lett* 404:98–110
- Connor CB, Connor LJ, Bonadonna C, Luhr JF, Savov I, Navarro-Ochoa C (2016) Modeling tephra thickness and particle size distribution of the 1913 eruption of Volcan de Colima. Mexico In press
- Cortés A, Macías JL, Capra L, Garduño-Monroy VH (2010) Sector collapse of the SW flank of Volcán de Colima, México. The 3600 yr BP La Lumbre-Los Ganchos debris avalanche and associated debris flows. *J Volcanol Geotherm Res* 197:52–66
- Costa A, Macedonio G (2005) Viscous heating effects in fluids with temperature-dependent viscosity: triggering of secondary flows. *J Fluid Mech* 540:21–38
- Costa A, Melnik O, Sparks RSJ (2007a) Controls of conduit geometry and wall-rock elasticity on lava dome eruptions. *Earth Planet Sci Lett* 260:137–151
- Costa A, Melnik O, Sparks RSJ, Voight B (2007b) Control of magma flow in dykes on cyclic lava dome extrusion. *Geophys Res Lett* 34(2)
- Costa A, Melnik O, Vedeneva E (2007c) Thermal effects during magma ascent in conduits. *J Geophys Res* 112:B12205
- Costa A, Sparks RSJ, Macedonio G, Melnik O (2009a) Effects of wall-rock elasticity on magma flow in dykes during explosive eruptions. *Earth Planet Sci Lett* 288:455–462
- Costa A, Caricchi L, Bagdassarov N (2009b) A model for the rheology of particle-bearing suspensions and partially molten rocks. *Geochem Geophys Geosyst* 10:Q03010
- Costa A, Gottsmann J, Melnik O, Sparks RSJ (2011) A stress-controlled mechanism for the intensity of very large magnitude explosive eruptions. *Earth Planet Sci Lett* 310:161–166
- De la Cruz-Reyna S (1993) Random patterns of activity of Colima Volcano, Mexico. *J Volcanol Geotherm Res* 55:51–68
- Diaz S (1906) Efemerides del Volcán de Colima, observaciones diarias desde los Observatorios de Zapotlan y Colima de 1893 a 1905. Sria De Fomento
- Dobran F (1992) Non-equilibrium flow in volcanic conduits and application to the eruptions of Mt. St. Helens on May 18, 1980 and Vesuvius in AD 79. *J Volcanol Geotherm Res* 49:285–311
- Eichelberger JC, Izbekov PE (2000) Eruption of andesite triggered by dike injection: contrasting cases at Karymsky Volcano, Kamchatka and Mt Katmai, Alaska. *Philos Trans R Soc Lond* 358: 1465–1485
- García-Pérez F, Urrutia-Fucugauchi J (1997) Crustal structure of the Arteaga Complex, Michoacán, southern Mexico, from gravity and magnetics. *Geof Intern Mexico* 36:235–244
- Gavilanes-Ruiz JC, Cuevas-Muñiz A, Varley N, Gwynne G, Stevenson J, Saucedo-Girón R, Pérez-Pérez A, Aboukhalil M, Cortés-Cortés A (2009) Exploring the factors that influence the perception of risk: the case of Volcán de Colima, Mexico. *J Volcanol Geotherm Res* 186: 238–252
- Giordano D, Russell JK, Dingwell DB (2008) Viscosity of magmatic liquids: a model. *Earth Planet Sci Lett* 271:123–134. <https://doi.org/10.1016/j.epsl.2008.03.038>
- Gudmundsson A, Brenner S (2005) On the conditions of sheet injections and eruptions in stratovolcanoes. *Bull Volcanol* 67(8):768–782. <https://doi.org/10.1007/s00445-005-0433-7>
- Gudmundsson A, Philipp SL (2006) How local stress fields prevent volcanic eruptions. *J Volcanol Geotherm Res* 158:257–268
- Gudmundsson A (2012) Strengths and strain energies of volcanic edifices: implications for eruptions, collapse calderas, and landslides. *Nat Hazards Earth Syst Sci* 12(7):2241–2258
- Hildreth W, Fierstein J (2000) Katmai volcanic cluster and the great eruption of 1912. *Geol Soc Am Bull* 112(10):1594–1620
- Huppert HE, Woods AW (2002) The role of volatiles in magma chamber dynamics. *Nature* 420:493–495
- Jaupart C, Allègre CJ (1991) Gas content, eruption rate and instabilities of eruption regime in silicic volcanoes. *Earth Planet Sci Lett* 102(3–4): 413–429
- Lavallée Y, Varley N, Alatorre-Ibargüenito MA, Hess KU, Kueppers U, Mueller S, Richard D, Scheu B, Spieler O, Dingwell DB (2012) Magmatic architecture of dome-building eruptions at Volcan de Colima (Mexico). *Bull Volcanol* 74(1):249–260
- Luhr JF, Carmichael IS (1980) The Colima volcanic complex, México: part I. Postcaldera andesites from Volcán Colima. *Contrib Mineral Petrol* 76:127–147
- Luhr JF, Carmichael IS (1981) The Colima volcanic complex, Mexico: part II. Late-quaternary cinder cones. *Contrib Mineral Petrol* 76:76–127
- Luhr JF, Carmichael ISE (1990) Petrological monitoring of cyclical eruptive activity at Volcán Colima, México. *J Volcanol Geotherm Res* 42:235–260
- Luhr JF (2002) Petrology and geochemistry of the 1991 and 1998–1999 lava flows from Volcan Colima. Mexico *J Volcanol Geotherm Res* 117:169–194
- Luhr JF, Navarro C, Connor CB, and Connor LJ (2006) The 1913 VEI-4 Plinian eruption of Volcan Colima, Mexico: Tephrochronology, petrology, and plume modeling. In *Eos, Transactions of the American Geophysical Union* 52, V43B-1786, San Francisco, CA
- Lundgren P, Casu F, Manzo M, Pepe A, Bernardino P, Sansosti E, Lanari R (2004) Gravity and magma induced spreading of Mount Etna volcano revealed by satellite radar interferometry. *Geophys Res Lett* 31(4)
- Macedonio G, Dobran F, Neri A (1994) Erosion processes in volcanic conduits and application to the AD79 eruption of Vesuvius. *Earth Planet Sci Lett* 121:137–152
- Macedonio G, Neri A, Marti J, Folch A (2005) Temporal evolution of flow conditions in sustained magmatic explosive eruptions. *J Volcanol Geotherm Res* 143:153–172
- Macías J, Arce J, Sosa G, Gardner JE, Saucedo R (2017) Storage conditions and magma processes triggering the 1818CE Plinian eruption of Volcán de Colima. *J Volcanol Geotherm Res* 340:117–129. <https://doi.org/10.1016/j.jvolgeores.2017.02.025>
- Maccacferri F, Bonafede M, Rivalta E (2011) A quantitative study of the mechanisms governing dike propagation, dike arrest and sill formation. *J Volcanol Geotherm Res* 208:39–50

- Martel C, Poussineau S (2007) Diversity of eruptive styles inferred from the microlites of Mt Pelee andesite (Martinique, Lesser Antilles). *J Volcanol Geotherm Res* 166(3–4):233–254
- Massaro S, Sulpizio R, Costa A (2018) Evolution of magma feeding system during a Plinian eruption: the case of Pomici di Avellino eruption of Somma-Vesuvius, Italy. *Earth Planet Sci Lett* 482:545–555
- Massaro S (2018) Investigation on physical mechanisms driving eruptive style transitions by means of geological data and geophysical modeling. Unpublished PhD Thesis, University of Bari
- Mastin LG, Guffanti M, Servranck R, Webley P, Barsotti S, Dean K, Durant A, Ewert JW, Neri A, Rose WI, Schneider D, Siebert L, Stunder B, Swanson G, Tupper A, Volentik A, Waythomas CF (2009) A multidisciplinary effort to assign realistic source parameters models of volcanic ash-cloud transport and dispersion during eruptions. *J Volcanol Geotherm Res* 186:10–12
- Medina-Martinez F (1983) Analysis of the eruptive history of the Volcán de Colima, Mexico (1560–1980). *Geof Intern* 22:157–178
- Melnik O, Sparks RSJ (1999) Non-linear dynamics of lava dome extrusion. *Nature* 402:37–41
- Melnik O (2000) Dynamics of two-phase conduit flow of high-viscosity gas-saturated magma: large variations of sustained explosive eruption intensity. *Bull Volcanol* 62:153–170
- Melnik O, Sparks RSJ (2002) Dynamics of magma ascent and lava extrusion at Soufrière Hills Volcano, Montserrat, in *The Eruption of the Soufrière Hills Volcano, Montserrat From 1995 to 1999*, edited by TH. Druitt and BP Kokelaar. *Mem Geol Soc Lond* 21:153–171
- Melnik O, Sparks RSJ (2005) Controls on conduit magma flow dynamics during lava dome building eruptions. *J Geophys Res* 110:B02209
- Melnik O, Sparks RSJ, Costa A, Barmin A (2008) Volcanic eruptions: cyclicity during lava dome growth. In: *Encyclopedia of complexity and systems science*, Meyers
- Melnik O, Costa A (2014) Dual-chamber-conduit models of non-linear dynamics behavior at Soufriere Hills Volcano, Montserrat. *The Eruption of Soufriere Hills Volcano, Montserrat from 2000 to 2010*. *Geol Soc London Mem* 39:61–69
- Mériaux C, Jaupart C (1995) Simple fluid dynamic models of volcanic rift zones. *Earth Planet Sci Lett* 136(3–4):223–240
- Moore GM, Carmichael ISE (1998) The hydrous phase equilibria (to 3 kbar) of an andesite and basaltic andesite from western Mexico: constraints on water content and conditions of phenocryst growth. *Contrib Mineral Petrol* 130:304–319
- Mora JC, Macías JL, Saucedo R, Orlando A, Manetti P, Vaselli O (2002) Petrology of the 1998–2000 products of Volcán de Colima, México. *J Volcanol Geotherm Res* 117:195–212. [https://doi.org/10.1016/S0377-0273\(02\)00244-5](https://doi.org/10.1016/S0377-0273(02)00244-5)
- Muskhlishvili N (1963) *Some basic problems in the mathematical theory of elasticity*. Noordhoff, Leiden, The Netherlands
- Nakada S, Shimizu H, Ohta K (1999) Overview of the 1990–1995 eruption at Unzen Volcano. *J Geophys Res* 89:1–22
- Navarro C, Cortes A (1993) Eruptive behavior of Colima volcano previous to Pelean-type eruptions with presence of active domes at the summit during XIX & XX centuries. An evaluation of its volcano hazard. Abstracts, first international workshop on environmental volcanology, 6, 15–17 November, Morelia Michoacan, Mexico
- Neri M, Acocella V, Behncke B (2004) The role of the Pemicana fault system in the spreading of Mt. Etna (Italy) during the 2002–2003 eruption. *Bull Volcanol* 66(5):417–430
- Nicholson RS, Gardner JE, Neal CA (2011) Variations in eruption style during the 1931 a.d. eruption of Aniakchak volcano, Alaska. *J Volcanol Geotherm Res* 207:69–82
- Norini G, Capra L, Groppelli G, Agliardi F, Pola A, Cortes A (2010) Structural architecture of the Colima volcanic complex. *J Geophys Res* 115:B12209
- Núñez-Cornú F, Nava FA, De la Cruz-Reyna S, Jiménez Z, Valencia C, García-Arthur R (1994) Seismic activity related to the 1991 eruption of Colima Volcano, Mexico. *Bull Volcanol* 56:228–237
- Ortiz SG (1944) *La Zona volcanica Colima del Estado de Jalisco*. Publicaciones de la Universidad de Guadalajara. Guadalajara, Mexico
- Paidoussis MP (2006) Wave propagation in physiological collapsible tubes and a proposal for a Shapiro number. *J Fluids Struct* 22:721–725
- Pinel V, Jaupart C (2005) Some consequences of volcanic edifice destruction for eruption conditions. *J Volcanol Geotherm Res* 145(1):68–80
- Plateaux R, Béthoux N, Bergerat F, Mercier de Lépinay B (2014) Volcano-tectonic interactions revealed by inversion of focal mechanisms: stress field insight around and beneath the Vatnajökull ice cap in Iceland. *Front Earth Sci* 2:9. <https://doi.org/10.3389/feart.2014.00009>
- Preece K, Gertisser R, Barclay J, Charbonnier SJ, Komorowski JC, Herd RA (2016) Transitions between explosive and effusive phases during the cataclysmic 2010 eruption of Merapi volcano, Java, Indonesia. *Bull Volcanol* 78:54
- Poland MP, Peltrier A, Bonforte A, Puglisi G (2017) The spectrum of persistent volcanic flank instability: a review and proposed framework based on Kilauea, Piton de la Fournaise, and Etna. *J Volcanol Geotherm Res* 339:63–80
- Reid ME, Keith TE, Kayen RE, Iverson NR, Iverson RM, Brien DL (2010) Volcano collapse promoted by progressive strength reduction: new data from Mount St. Helens. *Bull Volcanol* 72(6):761–766
- Reubi O, Blundy J (2008) Assimilation of plutonic roots, formation of high-K ‘exotic’ melt inclusions and genesis of andesitic magmas at Volcán de Colima, Mexico. *J Petrology* 49(12):2221–2243
- Ripepe M, Bonadonna C, Folch A, Delle Donne D, Lacanna G, Marchetti E, Höskuldsson A (2013) Ash-plume dynamics and eruption source parameters by infrasound and thermal imagery: the 2010 Eyjafjallajökull eruption. *Earth Planet Sci Lett* 366:112–121
- Rivalta E, Segall P (2008) Magma compressibility and the missing source for some dike intrusions. *Geophys Res Lett* 35:L04306. <https://doi.org/10.1029/2007GL032521>
- Rivalta E (2010) Evidence that coupling to magma chambers controls the volume history and velocity of laterally propagating intrusions. *J Geophys Res* 115:B07203
- Rivalta E, Taisne B, Bungler AP, Katz R (2015) A review of mechanical models of dike propagation: schools of thought, results and future directions. *Tectonophysics* 638:1–42
- Roverato M, Capra L, Sulpizio R, Norini G (2011) Stratigraphic reconstruction of two debris avalanche deposits at Colima Volcano (Mexico): insights into pre-failure conditions and climate influence. *J Volcanol Geotherm Res* 207(1):33–46
- Rubin AM (1995) Propagation of magma-filled cracks. *Ann Rev Planet Sci* 23:287–336
- Rutherford MJ, Hill PM (1993) Magma ascent rates from amphibole breakdown: an experimental study applied to the 1980–1986 Mount St. Helens eruptions. *J Geophys Res* 98:19667–19685
- Salzer JT, Nikkhoo M, Walter T, Sudhaus H, Reyes-Dávila G, Bretón-Gonzalez M, Arámbula R (2014) Satellite radar data reveal short-term pre-explosive displacements and a complex conduit system at Volcan de Colima, Mexico. *Front Earth Sci* 2:12
- Scandone R, Cashman KV, Malone SD (2007) Magma supply, magma ascent and style of volcanic eruption. *Earth Planet Sci Lett* 253:513–529. <https://doi.org/10.1016/j.epsl.2006.11.016>
- Shapiro AH (1977) Steady flow in collapsible tubes. *J Biomech Eng* 99:126–147
- Savov IP, Luhr JF, Navarro-Ochoa C (2008) Petrology and geochemistry of lava and ash erupted from Volcan Colima, Mexico, during 1998–2005. *J Volcanol Geotherm Res* 174:241–256
- Saucedo R, Macías JL, Sheridan MF, Bursik MI, Komorowski JC (2005) Modeling of pyroclastic flows of Colima Volcano, Mexico:

- implications for hazard assessment. *J Volcanol Geotherm Res* 139(1–2):103–115
- Saucedo R, Macías J, Gavilanes JC, Arce JL, Komorowski JC, Gardner JE, Valdez-Moreno G (2010) Eyewitness, stratigraphy, chemistry, and eruptive dynamics of the 1913 Plinian eruption of Volcán de Colima, México. *J Volcanol Geotherm Res* 191:149–166
- Saucedo R, Macías JL, Gavilanes JC, Arce JL, Komorowski JC, Gardner JE, Valdez-Moreno G (2011) Corrigendum to eyewitness, stratigraphy, chemistry, and eruptive dynamics of the 1913 plinian eruption of Volcan de Colima, Mexico. *J Volcanol Geotherm Res* 191:149–166
- Sigmarrsson O, Vlastelic I, Andreassen R, Bindeman I, Devidal JL, Moune S, Thordarson T (2011) Remobilization of silicic intrusion by mafic magmas during the 2010 Eyjafjallajökull eruption. *Solid Earth* 2(2): 271–281
- Sigmundsson F, Hreinsdóttir S, Hooper A, Arnadóttir T, Pedersen R, Roberts MJ, Geirsson H (2010) Intrusion triggering of the 2010 Eyjafjallajökull explosive eruption. *Nature* 468(7322):426–430
- Smith VC, Shane P, Nairn IA (2004) Reactivation of a rhyolitic magma body by new rhyolitic intrusion before the 15.8 ka Rotorua eruptive episode: implications for magma storage in the Okataina Volcanic Centre, New Zealand. *J Geol Soc* 161(5):757–772
- Sparks RSJ (1978) The dynamics of bubble formation and growth in magmas: a review and analysis. *J Volcanol Geotherm Res* 3:1–37
- Sparks RSJ, Young SR (2002) The eruption of Soufrière Hills volcano, Montserrat (1995–1999): overview of scientific results, in the eruption of the Soufrière Hills volcano, Montserrat from 1995 to 1999, edited by TH Druitt and BP Kokelaar. *Mem Geol Soc Lond* 21:45–69
- Spica Z, Perton M, Legrand D (2017) Anatomy of the Colima volcano magmatic system, Mexico. *Earth Planet Sci Lett* 459:1–13
- Spera F (2000) Physical properties of magma, in *Encyclopedia of Volcanoes*, edited by H. Sigurdsson, pp. 171–190, Academic, San Diego, Calif
- Sulpizio R, Zanella E, Macías JL, Saucedo R (2015) Deposit temperature of pyroclastic density currents emplaced during the El Chichón 1982 and Colima 1913 eruptions. *Geol Soc Lond Spec Publ* 396(1):35–49
- Sulpizio R, Lucchi F, Forni F, Massaro S, Tranne C (2016) Unravelling the effusive-explosive transitions and the construction of a volcanic cone from geological data: the example of Monte dei Porri, Salina Island (Italy). *J Volcanol Geotherm Res* 327:1–22
- Sulpizio R, Massaro S (2017) Influence of stress field changes on eruption initiation and dynamics: a review. *Front Earth Sci* 03. <https://doi.org/10.3389/feart.2017.00018>
- Suter M, Martínez MC, Martínez ML, Farrar E (1995) The Aljibes half-graben. Active extension at the boundary between the trans-Mexican volcanic belt and the basin and Range Province, Mexico. *GSA Bull* 107(6):627–641
- Swanson D, Holcomb RT (1999) Regularities in growth of the Mount St. Helens dacite dome 1980–1986. In: Fink JH (ed) *Lava flows and domes: emplacement mechanisms and hazards implications*. Springer Verlag, Berlin, pp 3–24
- Touloukian YS, Judd WR, Roy RF (1989) *Physical properties of rocks and minerals*, 548. Hemisphere, New York
- Urbina F, Camacho H (1913) La zona megaséismica Acambay-Tixmadeje, estado de México: conmovida el 19 de noviembre de 1912 (Vol. 32). Imprenta y fototipia de la Secretaría de fomento
- Varekamp JC (1993) Some remarks on volcanic vent evolution during plinian eruptions. *J Volcanol Geotherm Res* 54:309–318
- Vargas-Bracamontes DM, Alejandro Nava F, Reyes-Dávila Gabriel A (2009) Time-scale wavelet patterns related to the 1998–1999 eruptions of the Colima volcano, and their possible implications for eruption forecasting. *J Volcanol Geotherm Res* 184:271–284
- Voight B, Linde AT, Sacks IS, Mattioli GS, Sparks RSJ, Elsworth D, Young SR (2006) Unprecedented pressure increase in deep magma reservoir triggered by lava-dome collapse. *Geophys Res Lett* 33(3)
- Waitz P (1915) El estado actual de los volcanes de Mexico y la ultima erupcion del Volcan de Colima (1913). *Revista Volcanologica*:259–268
- Walter TR, Amelung F (2007) Volcanic eruptions following $M \geq 9$ megathrust earthquakes: implications for the Sumatra-Andaman volcanoes. *Geology* 35(6):539–542
- Walter TR (2011) Structural architecture of the 1980 Mount St. Helens collapse: an analysis of the Rosenquist photo sequence using digital image correlation. *Geology* 39(8):767–770
- Watt SFL, Pyle DM, Mather TA (2009) The influence of great earthquakes on volcanic eruption rate along the Chilean subduction zone. *Earth Planet Sci Lett* 277:399–407
- Williams SN, Self S (1983) The October 1902 plinian eruption of Santa Maria volcano, Guatemala. *J Volcanol Geotherm Res* 16:33–56
- Wilson L, Sparks RSJ, Walker GPL (1980) Explosive volcanic eruptions - IV. The control of magma properties and conduit geometry on eruption column behaviour. *Geophys J Astr Soc* 63:174–148
- Wylie JJ, Voight B, Whitehead JA (1999) Instability of magma flow from volatile dependent viscosity. *Science* 285:1883–1885
- Woods AW, Koyaguchi T (1994) Transitions between explosive and effusive eruptions of silicic magmas. *Letters to Nature* 370:641–644
- Woods AW, Cowan A (2009) Magma mixing triggered during volcanic eruptions. *Earth Planet Sci Lett* 288:132–137
- Yagi Y, Mikumo T, Pacheco J, Reyes G (2004) Source rupture process of the Tecomán, Colima, Mexico earthquake of 22 January 2003, determined by joint inversion of teleseismic body-wave and near-source data. *Bull Seismol Soc Am* 94(5):1795–1807
- Young T (1808) Hydraulic investigations, subservient to an intended Croonian Lecture on the motion of the blood. *Philos Trans R Soc Lond* 98:164–186
- Zellmer G, Annen C (2014) An introduction to magma dynamics. Dynamics of crustal magma transfer, storage and differentiation. Annen C and Zellmer G (eds), *Geol Soc London spec. Public* 304: 1–13
- Zobin VM, Gonzalez Amezcua M, Reyes Davila GA, Dominguez T, Cerda Chacon JC, Chavez Alvarez JM (2002) Comparative characteristics of the 1997-1998 seismic swarms preceding the November 1998 eruption of Volcan de Colima, Mexico. *J Volcanol Geotherm Res* 117:47–60
- Zamora-Camacho A, Espíndola JM, Reyes-Dávila G (2007) The 1997–1998 activity of Volcán de Colima, Western Mexico: some aspects of the associated seismic activity. *Pure Appl Geophys* 164:39–52